

Hybrid ultrasonic vibration and magnetic field assisted diamond cutting of titanium alloys

W.S. Yip¹, S. To ^{1,*} and Zhanwen Sun²

¹State Key Laboratory in Ultra-precision Machining Technology, Department of Industrial and Systems Engineering, The Hong Kong Polytechnic University, Hung Hom, Kowloon, Hong Kong Special Administrative Region

² State Key Laboratory of Precision Electronic Manufacturing Technology and Equipment, Guangdong University of Technology, Guangzhou, China

*corresponding author: sandy.to@polyu.edu.hk

Abstract

Ultrasonic assisted machining is commonly used for machining of difficult to cut materials especially for titanium alloys in ultra-precision machining (UPM). However, the tool movements in ultrasonic assisted machining unavoidably induce surface damages and side burrs on the machined surface, in which the problem remains unsolved. To address this issue, in this study, a magnetic field is introduced in ultrasonic assisted diamond cutting in order to minimize the surface damages induced by the ultrasonic tool, and consequently improve surface finishing of machined titanium alloys. In the experiments, ultrasonic assisted diamond cutting of titanium alloys was conducted in the presence of a magnetic field. The experimental results showed that the degree of material swelling intensified by the ultrasonic tool movements was significantly reduced and suppressed in the presence of magnetic field. The area of cutting scars induced by the cyclic movements of the ultrasonic tool was minimized by the influence of the magnetic field. Moreover, the error percentages of groove depth and width generated in the presence of a magnetic field were considerably reduced to 1.69% and 1.77% respectively. By superimposing a magnetic field into the ultrasonic assisted diamond cutting process, the drawbacks of ultrasonic vibration assistance, especially the formation of aggregated swollen materials and cutting scars, are minimized.

Keyword: Ultrasonic assisted machining; Magnetic field assistance; Ultra-precision machining; Titanium alloys; Surface damage

1. Introduction

Ultrasonic assisted machining has been reported to be an effective machining technology to enhance machining performance, especially in ultra-precision machining (UPM), aiming to dissipate cutting heat in the machining processes. Researchers applied ultrasonic assisted machining to machine of various difficult to cut materials with different surface patterns. Suzuki et al. [1] proposed a novel sculpturing method in micro/nano scale for hardened steel in order to fabricate different nano/micro patterns using elliptical vibration cutting; it was found that the cutting thickness of the nano/micro patterns could be greatly controlled after applying their ultrasonic assisted technique. Amini et al. [2] proposed ultrasonic vibration assisted turning to generate micro dimples. Their experimental results showed reductions in the average friction coefficient, wear rate, and surface roughness at a relatively large feedrate and adhesion between pin and workpiece surface. Zhang et al. [3] implemented microgroove turning using an ultrasonic elliptical vibration. Because of the cooling effect induced by the tool separation in every cycle of ultrasonic movement, the experimental results showed that the cutting force and surface roughness of machined groove were greatly reduced. Zou et al. [4] presented a comprehensive analysis of ultrasonic vibration assisted single point diamond turning of die steel. They found that the friction force between the tool flank face and the machined surface was reduced because of frequent tool separations from the chip root under the ultrasonic vibration, and diamond tool wear was significantly reduced. It has been scientifically reported that ultrasonic vibration assisted machining enables the delivery of a cooling effect at the location of tool/workpiece interface in machining processes.

Although machinability of materials processed by ultrasonic assisted machining is enhanced, machined burrs and scars are found on the machined surfaces and edges in ultrasonic assisted cutting. Cao et al. [5] applied ultrasonic vibration for the grinding of silicon carbide. They found that although the surface damage of brittle deformation of silicon carbide was improved by ultrasonic assistance, the machined surface showed irregular scar and ragged materials especially on the bottom and edge areas. Geng et al. [6] applied ultrasonic assisted machining on carbon fiber-reinforced plastics and successfully minimized the thermal damage of workpiece by reducing the maximum cutting temperature; also, using the similar technique, the delamination of fiber was reduced [7]. Lu et al. [8] applied high pressure coolant on ultrasonic assisted cutting of titanium alloys and they discovered that cutting temperature decreased and therefore surface quality increased. Zhang et al. [9] conducted an ultrasonic assisted scratching test of SiC ceramics using a diamond tool and found that the surface integrity of the scratching surface generated by ultrasonic assistance was better than that of conventional scratching. However, they also found that the machined surface was still composed of machined scars. The materials were removed by a plastic deformation mode with the superimposition of an individual cutting cycle induced by ultrasonic vibration, so the scratching surface displayed the sinusoidal motion of the diamond indenter. This is evidence of the complete elastic-plastic deformation and plastic removal in single scratching, leading to a slight level of aggregated burrs on the machined surface. Kim and Loh [10] investigated the machining characteristics of ultrasonic elliptical cutting using a single point diamond tool. They found that the cutting force of ultrasonic cutting was remarkably reduced, and even though the burrs were much shallower than that of conventional diamond cutting, the formation of burrs at the bottom and edge areas of machined

surface still existed. Therefore, the machining problem associated with the superimposition of plastic removal areas induced by ultrasonic tool cutting, remain unsolved.

Various machining technologies using magnetic field influences are recorded in the literature, and excellent machining outcomes have been reported for hybrid machining technologies. Fan et al. [11] conducted experiments involving magnetic assisted electrochemical machining by installing permanent magnets into the tool. They discovered that extra energy was offered to electrochemical machining by the magnetic field influences, that critical voltage decreased with the level of excited particles at the higher energy level, and that the electric flux was inclined to focus because of the regular alignment of magnetic moments of processing ions. Cheng et al. [12] found that by introducing a magnetic field into electrochemical machining to solve the problem of unstable spark discharge, which was uncontrolled when the machining depth increased, the electrolyte circulation was highly enhanced and contributed to an improvement of machining accuracy and material removal rate. Without requiring a complicated machining setup, the improvement of overall machining time in their studies reached 57.4% under the magnetic field influence. Joshi et al. [13] introduced a hybrid dry electrical discharge machining integrated with a pulsed magnetic field to improve machining performance. The pulsed magnetic field was supplied tangential to the electric field, offering increases in electron movement and level of plasma ionization. They successfully demonstrated an improvement in productivity of over 130%, nearly no tool wear in comparison to that of dry electrical discharge machining without using the magnetic field, and the quality of the machined surface was also uplifted. Yip and To [14] applied 0.02T magnetic field intensity to diamond cutting of titanium alloys and found that because of the formations of highly conductive chains composed of magnetic particles at the tool/workpiece interface, the thermal conductivity of titanium alloys increased and therefore the machining performance increased as well. A magnetic field is combined with other machining technology to offer unexpectable benefits to machining performance without altering the material composition or requiring complicated equipment. The machining performance of different machining technologies is considerably enhanced under the influence of a magnetic field.

With the concept of magnetic field effect in UPM, the positive influences of magnetic field are believed to benefit ultrasonic assisted machining. The integral effects of ultrasonic vibration and a magnetic field have been used in electric discharge machining [15–17]. However, there are rare studies of uses of the integral effects combining ultrasonic vibration and magnetic field on UPM. Therefore, in this study, we applied a magnetic field effect on the ultrasonic assisted machining in UPM for the first time. In this study, a magnetic field was applied to ultrasonic assisted turning to minimize the aggerated cutting scars commonly found in ultrasonic assisted cutting. This study contributes to uplifting machining performance in terms of surface quality in ultrasonic assisted machining with a magnetic field. In particular, it shows the capability of suppressing cutting scars, which is the most common machining drawback of ultrasonic vibration assisted machining.

2. Theory

The basic idea of proposed machining technology is the combination of the concepts of ultrasonic-assisted machining and magnetic field assisted machining to enhance the machinability of titanium alloys. In this hybrid machining approach, materials are removed by the coupled effects of the two technologies, thereby providing the unique advantages of suppressing cutting scar and better surface quality.

2.1 The positive influences of ultrasonic vibration on machining

During ultrasonic assisted machining, the tool rake face periodically breaks off contact with the chip root of the machined surface. The tool position and its velocity are governed by the equations:

$$x(t) = A \sin(\omega t) + V_{feed} t \quad (1)$$

$$v = \omega A \cos(\omega t) + V_{feed} \quad (2)$$

Where $x(t)$ and v are the instantaneous position and velocity of vibrated tool at time t respectively, A is the amplitude of the ultrasonic tool vibration, ω is the angular frequency equal to $2\pi f$, denoting f as the vibration frequency, and V_{feed} is the feed velocity. It is worth to note that, compared with the conventional diamond cutting, ultrasonic assisted machining provides a better lubrication condition in the cutting region. The diamond tool periodically contacts and departs the materials, in which case the accumulated heat can be more easily taken away by the flowing coolant. Thus, the better lubrication effectively avoids the thermal-chemical reactions in the cutting region, accordingly, improving the surface quality. In this study, the maximum velocity of diamond tool in the cutting direction is:

$$v = 2\pi f A + V_{feed} \quad (3)$$

where f is 80 kHz and A is the vibration amplitude of 1.25 μm were set in the experiments. The maximum cutting velocity in this case is 628 mm/s, which is much higher than the feed velocity. The higher cutting velocity of vibration-assisted machining can not only enhance the chip formation but also improve machining efficiency.

2.2 The magnetic field influence on diamond machining of titanium alloys

In the environment of an absence of a magnetic field, different magnetic particles in the carrier fluid are randomly positioned due to Van der Waals forces and dipole-dipole interactions [18]. The underlying principle for an increase of thermal conductivity of the carrier containing metal particles in a presence of a magnetic field is that, the magnetic particles inside the carriers are aligned under an application of external magnetic field because of receiving sufficient dipole energy to overcome the Van der Waals forces and dipole-dipole interactions. When the magnetic field is applied, the dipole moments are aligned with the direction of the applied magnetic field [19] because of sufficient energy for the magnetic particles. The magnetic particles will move and align with the direction of the applied magnetic field as the positive value of the magnetic susceptibility of metal particles. The aligned particles become short metal chains in which they are relatively

higher conductivity [20,21] than that of an individual metal particle, and therefore the heat transference of the carrier with metal particles is enhanced under a magnetic field.

In the environment of no magnetic field, the magnetic particles aggregate with each other due to the Van Der Waals forces and dipole-dipole interactions. The dipole-dipole interaction energy U_d is denoted as [22]:

$$U_d = - \frac{3(m_i \cdot d_{ij})(m_i - d_{ij})}{d_{ij}^5} - \frac{(m_i \cdot d_{ij})}{d_{ij}^3} \quad (4)$$

where d_{ij} is the distance between the magnetic particles i and j , m_i and m_j are the mass of the magnetic particles of i and j respectively. The effective attraction tendency between two magnetic particles is expressed as coupling constant L :

$$L = \frac{U_d(ij)}{k_B T} \quad (5)$$

where k_B is Boltzmann constant and T is the temperature respectively. U_d becomes large when a magnetic field is presented, causing an occurrence of magnetic particle migration and aggregation. The individual magnetic particles become chain structures consequently and they move in the direction parallel to the applied magnetic field, as a result, the thermal conductivity of the carrier increases as the formation of highly conductive metal chains for transferring heat [20]. Actually, the literature showed the evidence of enhancement of thermal conductivity of carriers with metal particles through the formation of metal chains under a magnetic field. Gavili et al. [23] conducted the numerical investigation and confirmed the effects of magnetic field on the heat transference of carriers containing magnetic particles. Also, Lajvardi et al. [22] experimentally showed a significant increase in the heat transfer coefficient of ferrofluid under a magnetic field and therefore the heat transfer of that carrier was enhanced under a magnetic field.

On the other hand, the magnetic particle migration happens for the formation of a metal chain of the carrier in a magnetic field. With the magnetic particle migration effect, the metal particles under a magnetic field enable to move and aggregate to become chains to increase the thermal conductivity of the interface. Actually, magnetic particle migration under a magnetic field is known as magnetophoresis, it refers to a phenomenon of magnetic particle movement in a nonmagnetic/magnetic fluid under a magnetic field. Recently, examinations on magnetophoresis for metallic particle migrations under a magnetic field have been extensively conducted. In a carrier with magnetic particles, magnetic particles are affected and deflected under

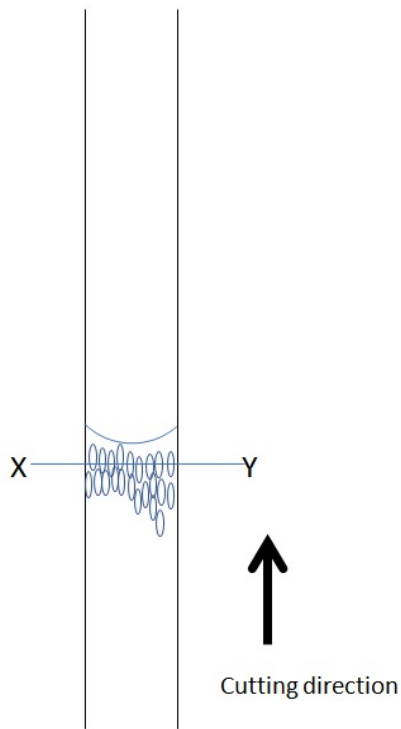
an external magnetic field relating to the magnetic susceptibility, magnetic field intensity and the speed of the carrier flow [24]. Therefore, the magnetic particle migration velocity V is denoted as [25]:

$$V = \frac{2r^2\pi\Delta\chi|B|\nabla|B|}{-9\mu_0\pi\eta} \quad (6)$$

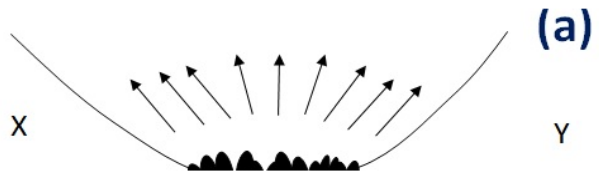
where r is the particle radius; $\Delta\chi$ is the difference between magnetic susceptibility of the particle and the carrier; B is magnetic induction; μ_0 is the permeability of free space; η is the viscosity of separation fluid. Therefore, when the materials contain the compositions with different magnetic susceptibility and suffer from magnetic field intensity in a media, magnetic particle migration will happen. For the case of UPM of titanium alloys under a magnetic field, as titanium alloys contain the elements of titanium, vanadium, aluminium, carbon and iron, which these elements have different magnetic susceptibility, and therefore the magnetic particle migration is expected to happen. In this article, the magnetic particles in the workpiece of the experiments were mainly titanium as it occupied the most for the titanium alloy workpiece. The evidence of metal particle migration would be shown in section “4.1 Evidence of magnetic field migration and the footprint” of this article.

2.3 The integral influences of ultrasonic vibration and magnetic field on machining

In UPM, materials recover in the random directions during solidification after machining processes [14]. In ultrasonic assisted UPM, the workpiece undergoes periodic pressure, strain and rising temperature from the ultrasonic assisted tool. Surfaces passed by an ultrasonic vibrated diamond tool, therefore, become an individual area for occurring material recovery in the solidification process. The recovered materials superimpose on each individual recovered area which can lead to obvious scars combining with random and ultrasonic vibration directions on the finished surfaces, as shown in Figure 1. In this study, through conducting the vibration-assisted machining under a magnetic field, the material removal mechanism can be changed by the magnetic field. Specifically, the magnetic field can suppress the material recovery by the formation of the metal chains through accelerating the magnetic particle migration into the bottom surfaces during each cutting cycle of vibration assisted machining, as discussed in the theory part. The illustration of the minimization of cutting scars by a magnetic field is shown in Figure 2.



The machined surface generated in every tool pass by an ultrasonic vibrated tool becomes an individual area for occurring material recovery in the solidification process, materials recover in the random direction in the solidification and they superimposed with each individual recovered area.



Materials are grown and expanded in the random direction and aggregated, the ragged areas finally become scars on the machining surface and edges

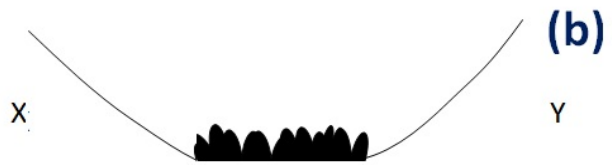
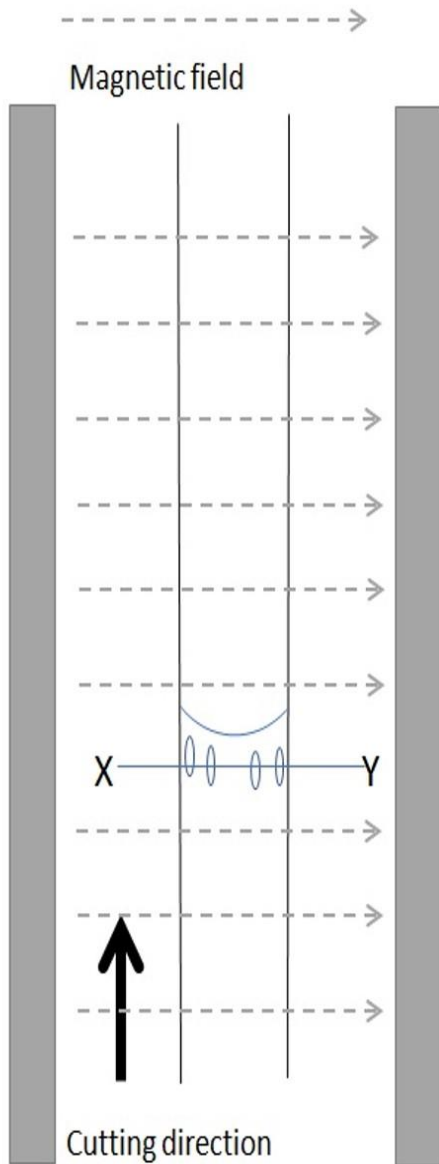
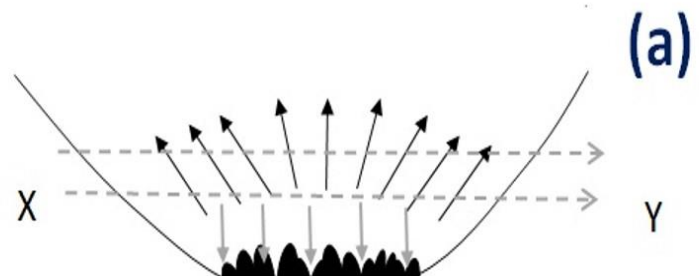


Figure 1(a-b). The formations of cutting scars on the machined surface induced by an ultrasonic assisted tool



The machines surface generated in tool pass by an ultrasonic vibrated tool becomes an individual area for material recovery.



The expansion of materials is suppressed, leaving less height of the ragged areas, removing the cutting scars on the machining surface and edges

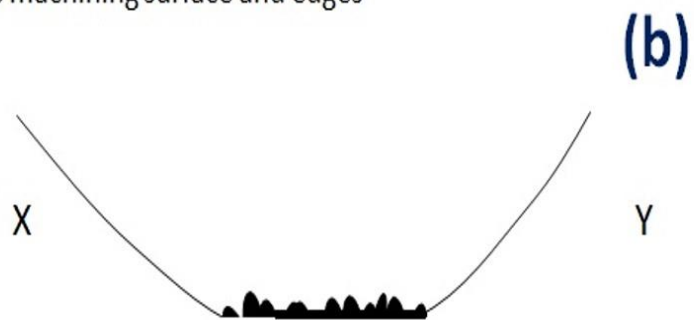


Figure 2(a-b). The reduction of cutting scars on the machined surface induced by an ultrasonic assisted tool under a magnetic field

3. Experimental Setup

A two-phase titanium alloy, Ti6Al4V(TC4), was used as the material for the experiments. A single point diamond tool was installed on top of the ultrasonic device sonx-uts one system, which provided a vibration frequency of 80kHz with amplitude of $1.25\mu\text{m}$ to the diamond tool during the cutting processes. The ultrasonic vibration direction was parallel to the cutting direction. Straight lines were cut on the titanium alloy's surface using the ultrasonic assisted tool in the presence and absence of a magnetic field. Comparison tests were also conducted by using a normal diamond tool without adding ultrasonic vibration in the absence of a magnetic field. The cutting parameters and tool specification were: depth of cut $6\mu\text{m}$ and $7\mu\text{m}$, feedrate (cutting velocity) 150 mm/min, and tool radius 1.114mm. Therefore, 6 individual grooves were generated on the titanium alloy's surface. The machined grooves generated by an ultrasonic assisted diamond tool in the presence of magnetic

field, ultrasonic assisted diamond tool in the absence of magnetic field, and a normal diamond tool without an ultrasonic vibration assistance in the absence of magnetic field were named as UAMFS (ultrasonic assisted magnetic field sample), UAS (ultrasonic assisted sample) and NDCS (normal diamond cutting sample) respectively. A magnetic field with magnetic field intensity of 0.02T was provided by two permanent magnets. The titanium alloy samples were placed at the center of two permanent magnets for exposure to a magnetic field. The experimental setup of ultrasonic assisted diamond cutting in the presence of magnetic field is shown in Figure 3. A Moore Nanotech 350FG, 4 axis Ultra-precision machine was used for implementing the diamond cutting tests, and a non-contact optical profiling system (Wyko NT8000) was used to measure the groove profile and surface roughness of the samples. The cutting scars on the machined surface were observed by a scanning electron microscope (Hitachi HT3030).

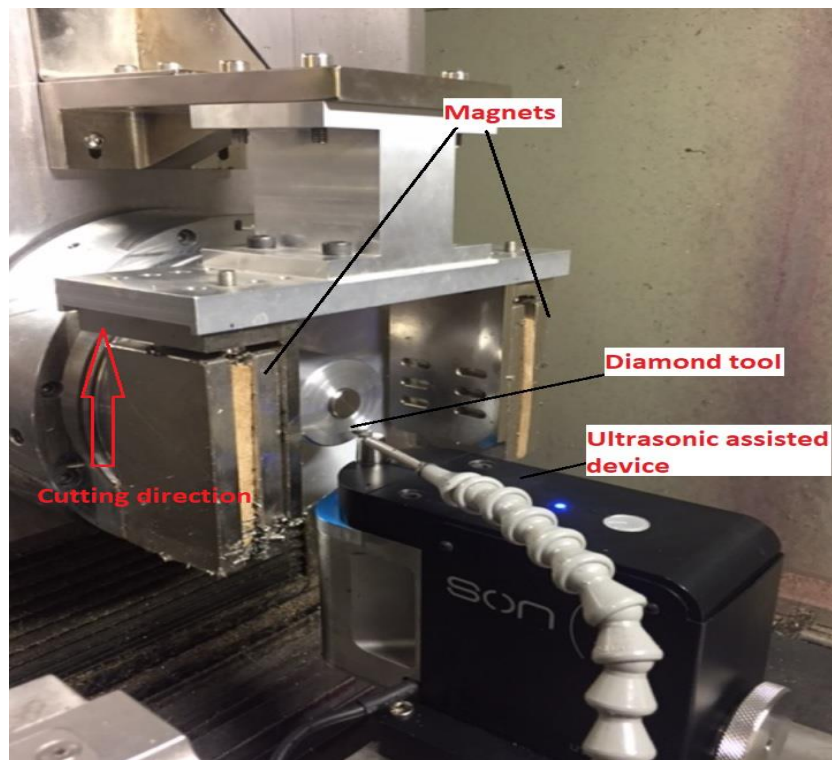


Figure 3. Experimental setup of ultrasonic assisted diamond cutting in the presence of magnetic field

4. Results and discussion

4.1 Evidence of magnetic field migration and the footprint

The measured 3D surface topology of NDCSs, UASs and UAMFSs is shown in Figures 4. The figure shows material recovery on the bottom areas of machined surfaces. NDCSs showed recovered materials and ragged marks on the surfaces with the direction parallel to the main cutting direction. After adding an ultrasonic vibration on the diamond tool, UASs show cutting marks with vibration footprints on the machined surface with the direction parallel to the main cutting and tool vibration directions. Under the influence of ultrasonic vibration, the diamond tool moved forward and backward in the main cutting direction, thereby creating worn and muddled areas in between each cutting mark generated by the main cutting motion on the UASs and

showing the effectiveness of the stirring effect from the ultrasonic assisted tool on the material recovery surface, as illustrating by Figure 1. For the surface topology of UAMFSs, the cutting marks, which appeared in both NDCSs and UASs, were minimized. On the contrary, the metallic marks with the parallel directions of magnetic field directions were shown in UAMFSs, as shown in Figure 4. The metallic marks acted as evidence of magnetic particle migration in ultrasonic assisted diamond cutting in a presence of magnetic field. Because of the horizontal migration of magnetic particles during the ultrasonic assisted cutting in the presence of magnetic field, the magnetic particle chains were formed, which demonstrated as the linear ragged shapes appearing on the machined surfaces, shown as white squared in Figure 4. With the linear metal chain forming for increasing heat transference at the cutting interface, the material recovery on the machined surface was minimized. On the other hand, the horizontal footprint induced by the magnetic field influence added to the main cutting marks, and therefore the footprint of tool mark generated from diamond cutting was averaged and blurred, causing the reduction of the vertical cutting marks and random material swelling induced by the ultrasonic tool motion. The horizontal footprint on the machined surface of UAMFSs provides solid evidence that the movement of magnetic particles is in the direction of the applied magnetic field in the ultrasonic assisted diamond cutting process.

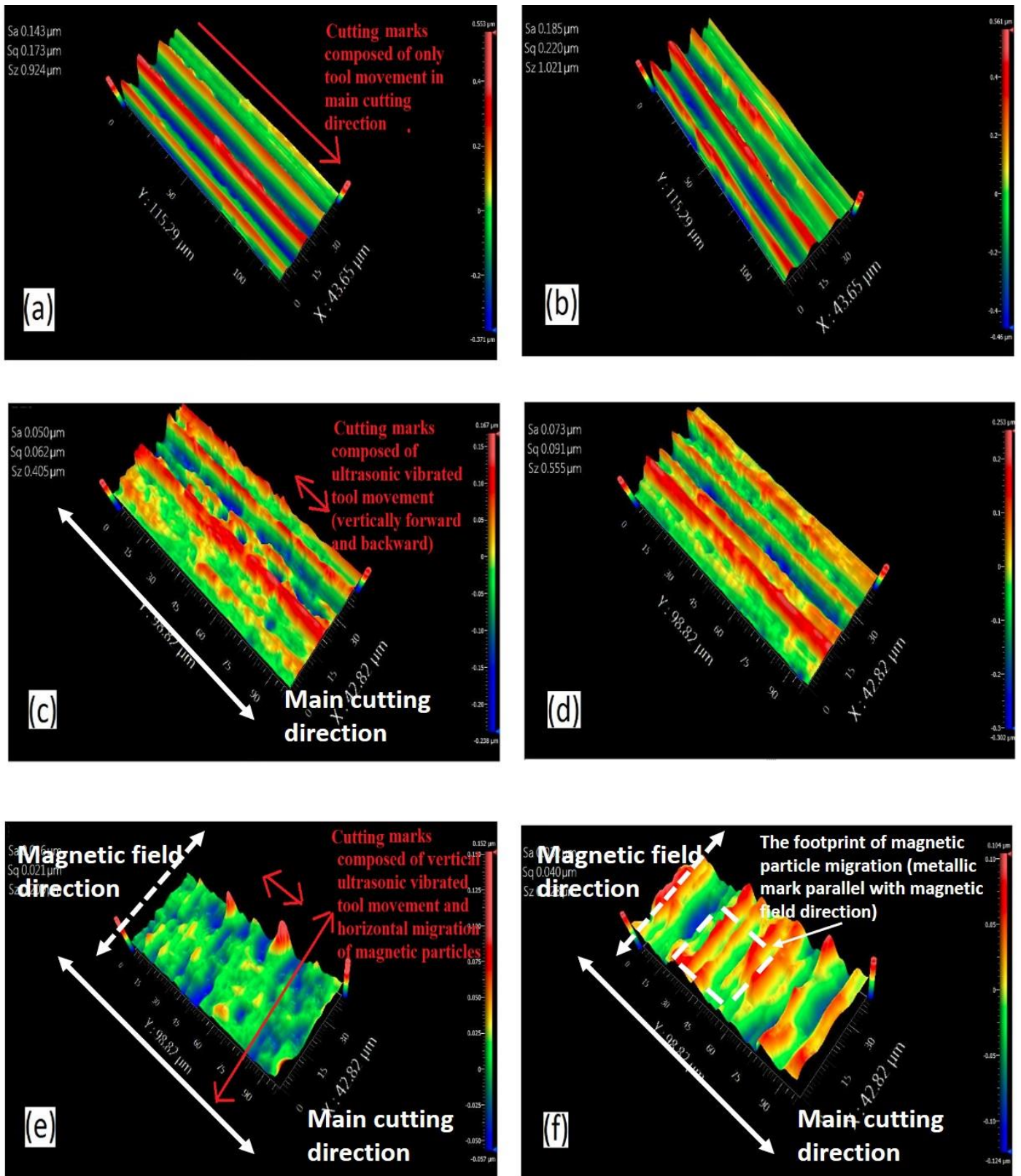


Figure 4. 3D surface topography of (a)NDCS at depth of cut 6μm, (b) NDCS at depth of cut 7μm, (c) UAS at depth of cut 6μm, (d) UAS at depth of cut 7μm, (e) UAMFS at depth of cut 6μm and (f) UAMFS at depth of cut 7μm

4.2 Surface analysis

With the demonstration of the footprint of magnetic particle migration and formation of metallic chains on the surface in ultrasonic assisted UPM, the surface quality is expected to increase for UAMFS. In order to remove the abrasive particles on the samples surfaces which were generated from the machining processes, two

cleaning steps were conducted. Firstly, the samples were cleaned with cleaning solution and a cotton swab to remove excess abrasive particles. Secondly, the samples were cleaned by an ultrasonic cleaner with cleaning solution. Therefore, it is ensured that no impurity was on the sample surfaces during the measurement. According to Figures 5, the machined surfaces of NDCSs at depth of cut $6\mu\text{m}$ and $7\mu\text{m}$ showed obvious vertical swelling marks, and the recovered materials were expanded at the bottom areas of the grooves parallel to the main cutting direction. For the machined surface of UASs, however, this is because the cutting marks were generated from every cutting cycle of ultrasonic assisted tool on the machined surface so that the recovered materials were superimposed to other recovered materials in a random direction. As a result, the aggregated cutting scars were formed on the bottom of the machined groove, which severely deteriorated the surface quality of the machined surface. Moreover, burrs were generated on the groove edge as shown in Figures 6(a-b). The materials were recovered elastically at the groove edge in every tool pass of ultrasonic vibrated tool and aggregated at that location, showing as uncut materials and remaining at the edges. On the contrary, for the UAMFSs, the machined surfaces were smooth and non-wavy, the cutting scars generated by the ultrasonic vibrated scar were reduced, displaying a crack free wavy surface. Also, UAMFSs demonstrated better surface finishing at the groove edges as shown in Figures 6(c-d), with only an extremely small amount of materials attached to the edges that did not aggregate and form as a burr. The above experimental results provide evidence of improvement of surface finishing under a magnetic field, and the ability to smooth cutting scars generated by the ultrasonic vibrated tool.

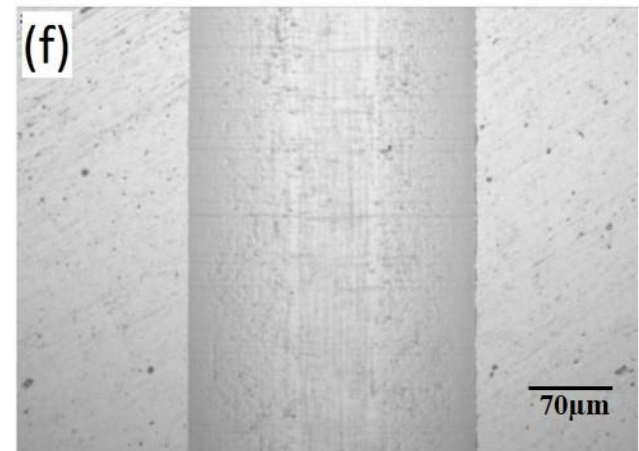
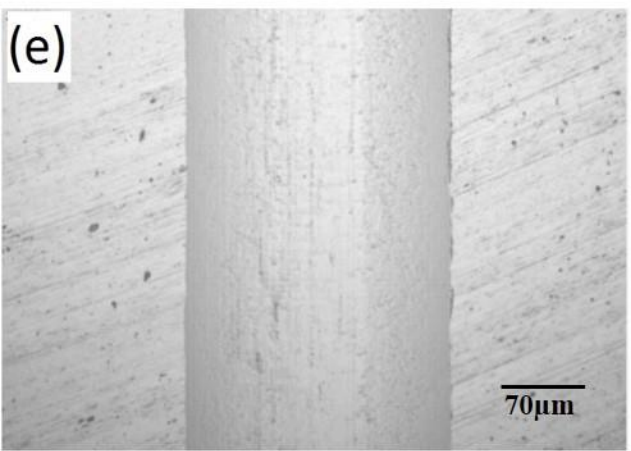
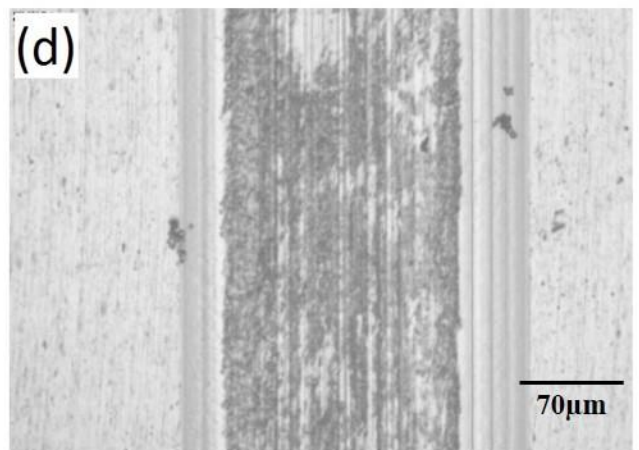
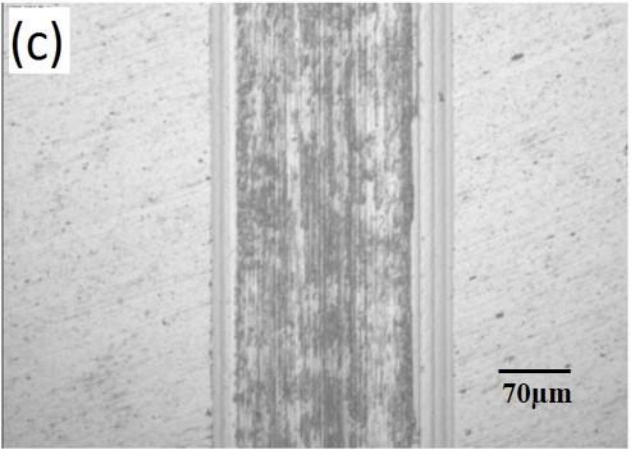
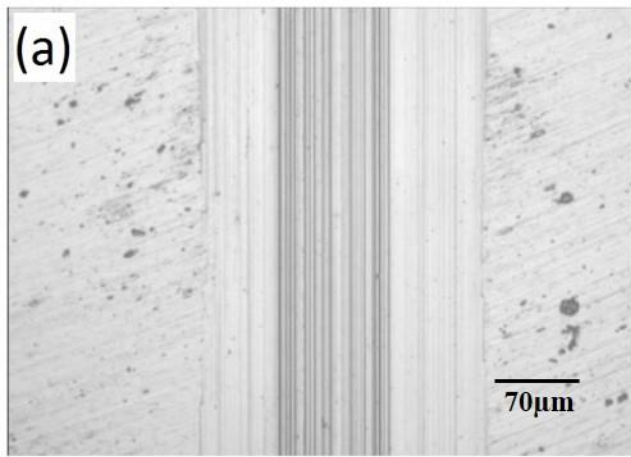


Figure 5. The microscope of (a) NDCS at depth of cut $6\mu\text{m}$, (b) NDCS at depth of cut $7\mu\text{m}$, (c) UAS at depth of cut $6\mu\text{m}$, (d) UAS at depth of cut $7\mu\text{m}$, (e) UAMFS at depth of cut $6\mu\text{m}$ and (f) UAMFS at depth of cut $7\mu\text{m}$

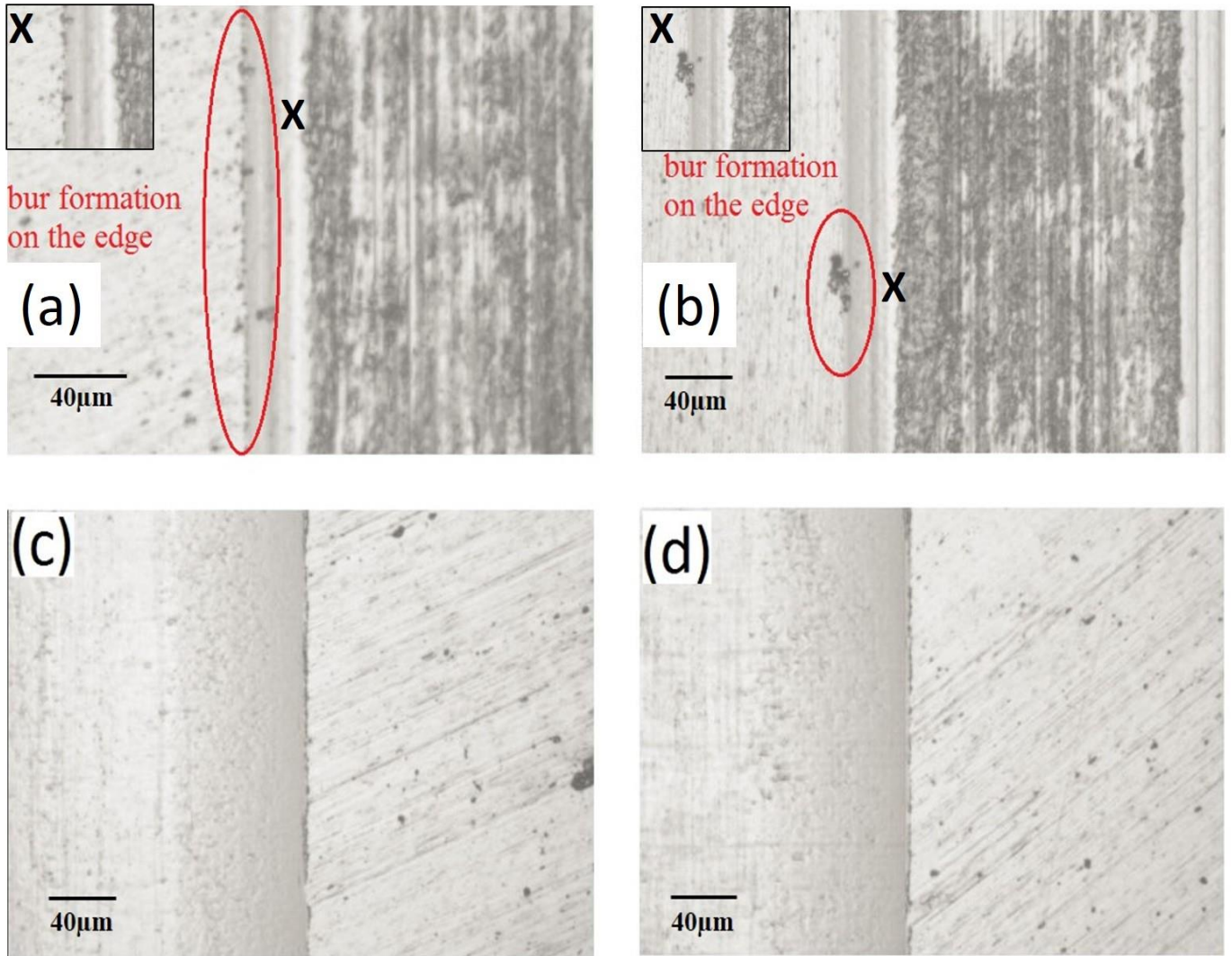
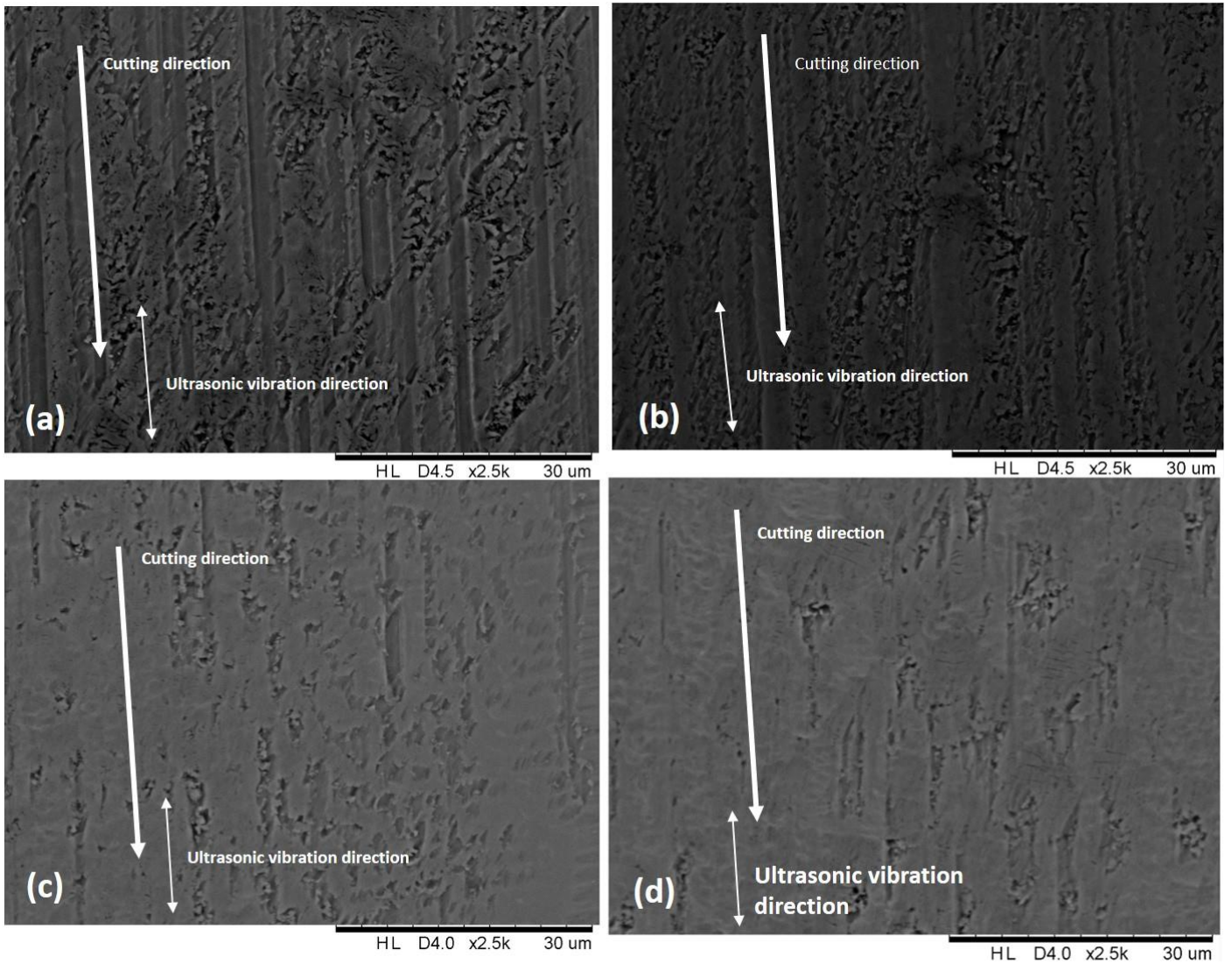


Figure 6. Microscope of the machined edges of (a) UAS at depth of cut 6µm with clear view of area x, (b) UAS at depth of cut 7µm with clear view of area x, (c) UAMFS at depth of cut 6µm and (d) UAMFS at depth of cut 7µm

In order to observe clearly the structure of cutting scars generated by the ultrasonic assisted tool on the machined surface with and without a magnetic field, SEM of UASs and UAMFSs were obtained and shown in Figures 7. Apparently, the size and the area of cutting scars on UASs were much larger than that of UAMFSs. For UASs, the cutting scars showed almost everywhere on the surface, the distribution of those cutting scars was parallel to the direction of the main cutting distance, showing the evidence of aggregated material recovery in the main cutting direction. On the contrary, for UAMFSs, the size and the number of cutting scars generated by the ultrasonic vibrated tool were reduced lots. The length of vertical scars showed shorter than that of UASs. Only a few surface areas were covered with cutting scars.



Figures 7. SEM of (a) UAS at depth of cut $6\mu\text{m}$, (b) UAS at depth of cut $7\mu\text{m}$, (c) UAMFS at depth of cut $6\mu\text{m}$ and (d) UAMFS at depth of cut $7\mu\text{m}$

4.3 Surface profile and form accuracy

The surface profiles of machined groove NDCSs, UASs and UAMFSs were measured and are shown in Figure 8. According to the figure, the machined profiles of NDCSs were distorted to a large degree, the entire groove shape is extremely wavy, especially the bottom area. The surface bottom displayed distinctive and clear crests and valleys as shown by red circle in Figure 8(a), which was consistent with the results of 3D surface topology indicating the cutting marks on the surface. For the machined profiles of UASs, although ultrasonic vibration was added to the diamond tool to deliver the cooling effect at the tool/workpiece interface, the entire groove shape was still distorted. The groove profiles were ragged and tattered. The forward and backward movements of the ultrasonic assisted tool caused random scars on the machined surface, leading to distinctive and obvious crests and valleys. On the contrary, UAMFSs machined profiles showed smooth and complete shapes, which were fit for the cutting tool profile. The edge and bottom areas of the machined grooves of UAMFSs showed as being flat without distortive ragged materials. The magnetic field influence again offered the suppression

of wavy and ragged surface induced by an unavoidable material recovery in ultrasonic assisted diamond cutting of titanium alloys.

The degree of material recovery can be shown by the difference between the assigned depth of cut and actual groove depth, and the difference between the cutting width and groove width. This information is shown in Tables 1 and 2 where it can be seen that the error percentages of groove depth and width for NDCSs were extremely large at 757.14% and 22.66% respectively. The volume and height of recovered material occupied over half of that of removed material. On the other hand, the error percentage of groove depth was larger than that of groove width, indicating that material recovery at the bottom area was much more serious than that of the side area in diamond cutting. For UASs, a sole application of ultrasonic vibration to the tool only improved surface accuracy to a very limited extent, and although the error percentages of groove shape improved slightly, they are still 114.29% for groove depth and 5.02% for groove width. Conversely, the error percentages of both groove depth and width for UAMFSs were minimized to a large extent with their values reduced to 7.69% and 3.75% respectively.

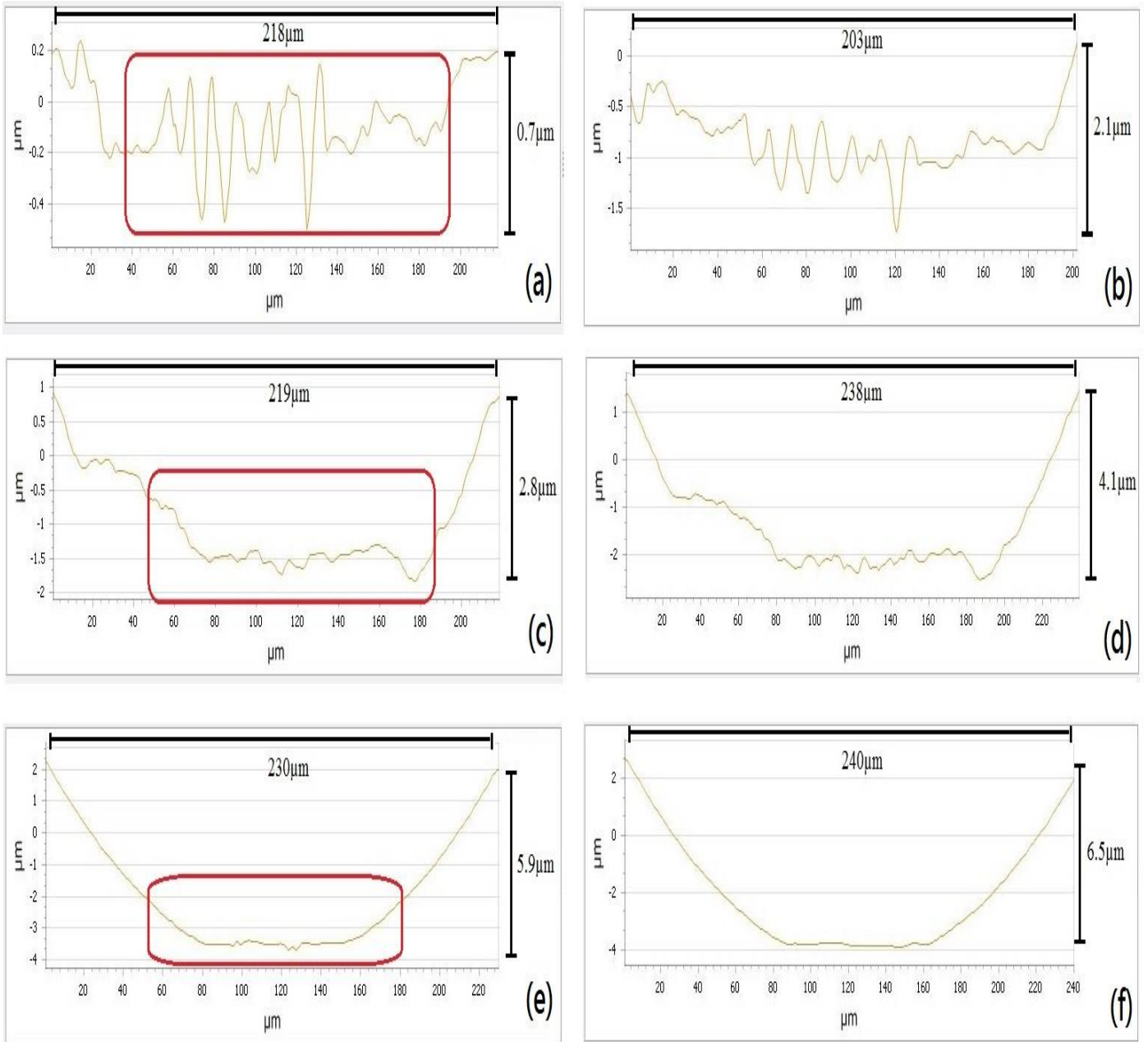


Figure 8. The surface profiles of (a) NDCS at depth of cut 6 μm , (b) NDCS at depth of cut 7 μm , (c) UAS at depth of cut 6 μm , (d) UAS at depth of cut 7 μm , (e) UAMFS at depth of cut 6 μm and (f) UAMFS at depth of cut 7 μm

Table 1. Assigned depth of cut, actual groove depth and the error percentages of NDCSs, UASs and UAMFSs

Assigned depth of cut (μm)	Groove depth(μm)			Error percentage		
	NDCS	UAS	UAMFS	NDCS	UAS	UAMFS
6	0.7	2.8	5.9	757.14	114.29	1.69
7	2.1	4.1	6.5	233.33	70.73	7.69

Table 2. Cutting width, groove width and the error percentages of NDCSs, UASs and UAMFSs

Assigned cutting width (μm)	Groove width			Error percentage		
	NDCS	UAS	UAMFS	NDCS	UAS	UAMFS
230	218	219	226	5.50	5.02	1.77
249	203	238	240	22.66	4.62	3.75

5. Conclusion

In response to the issue of heat transference in diamond cutting of titanium alloys, previous studies have recommended an application of ultrasonic assisted diamond cutting to provide a cooling effect induced from tool separations by an ultrasonic vibrated tool, which lowers cutting temperature at the tool/workpiece interface and thus reduces the degree of material recovery. However, the drawback of the ultrasonic assisted technique is that the cutting scars generated by every tool pass in ultrasonic cutting cycle are inevitably left on the machined surface, which counteracts the positive influence of ultrasonic assisted cutting on machining performance. In this study, in response to the problematic material recovery and the generation of cutting scars by an ultrasonic assisted diamond tool, a magnetic field is introduced into ultrasonic assisted diamond cutting of titanium alloys to resolve the above underlying sources of deteriorating surface quality.

Acknowledgment

General Research Fund from the Research Grants Council of Hong Kong Special Administrative Region under the project code PolyU 152125/18E.

References

- [1] Suzuki N, Yokoi H, Shamoto E. Micro/nano sculpturing of hardened steel by controlling vibration amplitude in elliptical vibration cutting. *Precis Eng* 2011;35:44–50.
- [2] Amini S, Hosseinabadi H N, Sajjady S A. Experimental study on effect of micro textured surfaces generated by ultrasonic vibration assisted face turning on friction and wear performance. *Appl Surf Sci* 2016;390:633–48.
- [3] Zhang C, Guo P, Ehmann K F, Li Y. Turning of microgrooves both with and without aid of ultrasonic elliptical vibration. *Mater Manuf Process* 2015;30:1001–9.
- [4] Zou L, Huang Y, Zhou M, Duan L. Investigation on diamond tool wear in ultrasonic vibration-assisted turning die steels. *Mater Manuf Process* 2017;32:1505–11.
- [5] Cao J, Wu Y, Lu D, Fujimoto M, Nomura M. Material removal behavior in ultrasonic-assisted scratching of SiC ceramics with a single diamond tool. *Int J Mach Tools Manuf* 2014;79:49–61.
- [6] Geng D, Lu Z, Yao G, Liu J, Li Z, Zhang D. Cutting temperature and resulting influence on machining performance in rotary ultrasonic elliptical machining of thick CFRP. *Int J Mach Tools Manuf* 2017;123:160–70.
- [7] Geng D, Liu Y, Shao Z, Zhang M, Jiang X, Zhang D. Delamination formation and suppression during rotary ultrasonic elliptical machining of CFRP. *Compos Part B Eng* 2020;183:107698.
- [8] Lu Z, Zhang D, Zhang X, Peng Z. Effects of high-pressure coolant on cutting performance of high-speed ultrasonic vibration cutting titanium alloy. *J Mater Process Technol* 2020;279:116584.
- [9] Zhang C, Feng P, Zhang J. Ultrasonic vibration-assisted scratch-induced characteristics of C-plane sapphire with a spherical indenter. *Int J Mach Tools Manuf* 2013;64:38–48.
- [10] Kim G D, Loh B G. Direct machining of micro patterns on nickel alloy and mold steel by vibration assisted cutting. *Int J Precis Eng Manuf* 2011;12:583–8.
- [11] Fan Z, Wang T, Zhong L. The mechanism of improving machining accuracy of ECM by magnetic field. *J Mater Process Technol* 2004;149:409–13.
- [12] Cheng C-P, Wu K-L, Mai C-C, Hsu Y-S, Yan B-H. Magnetic field-assisted electrochemical discharge machining. *J Micromechanics Microengineering* 2010;20:75019.
- [13] Joshi S, Govindan P, Malshe A, Rajurkar K. Experimental characterization of dry EDM performed in

a pulsating magnetic field. *CIRP Ann Technol* 2011;60:239–42.

- [14] Yip W S, To S. Reduction of material swelling and recovery of titanium alloys in diamond cutting by magnetic field assistance. *J Alloys Compd* 2017;722. <https://doi.org/10.1016/j.jallcom.2017.06.167>.
- [15] Zhang Z, Huang H, Ming W, Xu Z, Huang Y, Zhang G. Study on machining characteristics of WEDM with ultrasonic vibration and magnetic field assisted techniques. *J Mater Process Technol* 2016;234:342–52.
- [16] Wang Y, Wang Q, Ding Z, He D, Xiong W, Chen S, et al. Study on the mechanism and key technique of ultrasonic vibration and magnetic field complex assisted WEDM-LS thick shape memory alloy workpiece. *J Mater Process Technol* 2018;261:251–65.
- [17] Singh G, Satsangi P S, Prajapati D R. Effect of Rotating Magnetic Field and Ultrasonic Vibration on Micro-EDM Process. *Arab J Sci Eng* 2020;45:1059–70.
- [18] Gavili A, Zabihi F, Isfahani T D, Sabbaghzadeh J. The thermal conductivity of water base ferrofluids under magnetic field. *Exp Therm Fluid Sci* 2012;41:94–8.
- [19] Rosensweig R E. *Ferrohydrodynamics*. Courier Corporation; 2013.
- [20] Philip J, Shima P D, Raj B. Evidence for enhanced thermal conduction through percolating structures in nanofluids. *Nanotechnology* 2008;19:305706.
- [21] Nkurikiyimfura I, Wang Y, Pan Z. Heat transfer enhancement by magnetic nanofluids: A review. *Renew Sustain Energy Rev* 2013;21:548–61.
- [22] Lajvardi M, Moghimi-Rad J, Hadi I, Gavili A, Isfahani T D, Zabihi F, et al. Experimental investigation for enhanced ferrofluid heat transfer under magnetic field effect. *J Magn Mater* 2010;322:3508–13.
- [23] Gavili A, Lajvardi M, Sabbaghzadeh J. The effect of magnetic field gradient on ferrofluids heat transfer in a two-dimensional enclosure. *J Comput Theor Nanosci* 2010;7:1425–35.
- [24] Pamme N, Manz A. On-chip free-flow magnetophoresis: continuous flow separation of magnetic particles and agglomerates. *Anal Chem* 2004;76:7250–6.
- [25] Alnaimat F, Dagher S, Mathew B, Hilal-Alnqbi A, Khashan S. Microfluidics based magnetophoresis: A review. *Chem Rec* 2018;18:1596–612.